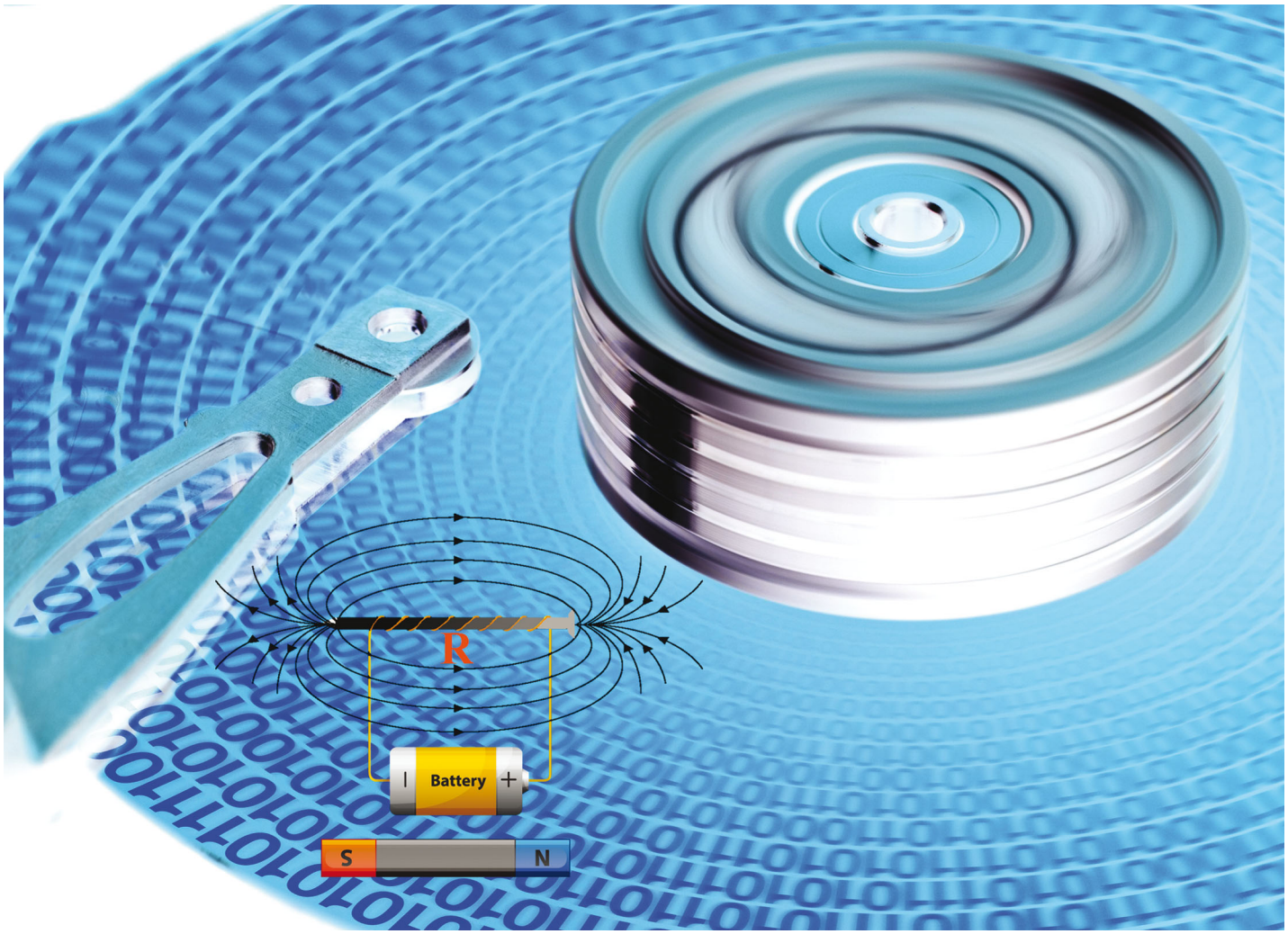

Showcasing research from the Chemical Science and Technology at Tongji University

Controllable organic magnetoresistance in polyaniline coated poly(*p*-phenylene-2,6-benzobisoxazole) short fibers

A tunable organic magnetoresistance (OMAR) effect in polyaniline (PANI) coated acid treated poly(*p*-phenylene-2,6-benzobisoxazole) (t-PBO) short fibers.

As featured in:

See Hongbo Gu *et al.*, *Chem. Commun.*, 2019, **55**, 10068.

ROYAL SOCIETY OF CHEMISTRY | Celebrating IYPT 2019

rsc.li/chemcomm

Registered charity number: 207890

ChemComm

COMMUNICATION

View Article Online
View Journal | View Issue

Check for updates

Cite this: *Chem. Commun.*, 2019, 55, 10068

Received 22nd June 2019,
Accepted 8th July 2019

DOI: 10.1039/c9cc04789a

rsc.li/chemcomm

Published on 09 July 2019. Downloaded on 9/26/2019 8:19:21 PM.

Controllable organic magnetoresistance in polyaniline coated poly(*p*-phenylene-2,6-benzobisoxazole) short fibers†

Hongbo Gu, *[a] Xiaojiang Xu,[a] Jingyi Cai,[a] Suying Wei,[b] Huige Wei,[bc] Hu Liu,[de] David P. Young,[f] Qian Shao,[g] Shide Wu,[h] Tao Ding[i] and Zhanhu Guo[d]

Herein, we first report a tunable organic magnetoresistance (OMAR) effect in polyaniline (PANI) coated acid treated poly(*p*-phenylene-2,6-benzobisoxazole) (t-PBO) short fibers. This unique OMAR is interpreted using the paramagnetic nature of PBO molecules combined with the localization length a_0 calculated from the wave-function shrinkage model and forward interference model.

Giant magnetoresistance (GMR), as the birth of spintronics, is a quantum mechanical effect that is related to different spin energy states of electrons at the Fermi level arising from spin splitting between spin-up and spin-down electrons after applying an external magnetic field.[1] Recently, due to the weak spin–orbit coupling and hyperfine interaction of carbon, organic semiconductors have been considered as new spintronic materials.[2,3] As a result, they are also recognized as having organic magnetoresistance (OMAR) and as organic spintronics.[4] In general, the OMAR phenomenon is associated with the paramagnetic species in the organic semiconductors including electrons and holes, triplet excitons, or bipolarons.[5] Correspondingly, the mechanism of the OMAR effect is commonly explained by the electron–hole (e–h) recombination model,[6] excitonic pair mechanism model,[7] and bipolaron model.[8] Polyaniline (PANI) is one of the most investigated conducting polymers in applications such as anti-fog coatings, supercapacitors, energy and environmental remediation due to its low cost, easy synthesis process, environmental stability, high electrical conductivity and high pseudo capacitance.[9,10] For example, Gu *et al.*[11] discussed the electrical transport in disordered PANI nanostructures and critically reviewed the recently discovered OMAR phenomenon in PANI and its nanocomposite systems. They not only observed positive OMAR in PANI systems,[12,13] but also reported a unique high negative OMAR in $CoFe_2O_4$/PANI nanocomposites.[14] The addition of different nanofillers could significantly alter the OMAR effect of PANI by enhancing or reducing its OMAR values.[15]

High-performance poly(*p*-phenylene-2,6-benzobisoxazole) (PBO) is a heterocyclic aromatic polybenzoxazole with rigid-rod conjugated molecular configurations, where the conjugated benzoxazole and phenyl rings in its polymer backbone lead to an extended π electron delocalization.[16] Therefore, it has many outstanding properties like mechanical properties[17] and dielectric properties[18] as well as thermal stability and photoluminescent properties.[19] PBO fibers can be applied in organic light-emitting diodes, electroluminescent devices and textiles such as firefighters' protective clothing, bullet-proof vests, and cables requiring stiffness and strength in tension as an ideal reinforcement.[20,21] Nevertheless, the lack of functional groups on the surface of PBO fibers makes them chemically inert. Accordingly, surface treatment, including oxidation, plasma treatment, physical radiation and so on,[22] of PBO fibers is commonly required to achieve a good compatibility and adhesion with the polymer matrix. Moreover, it is reported that PBO polymer structures possess intrinsic paramagnetic properties. It would be interesting to explore the possible OMAR effect in composites composed of PBO fibers and PANI. However, there is no related report yet.

In this work, we comprehensively investigate the OMAR effect in PANI coated acid treated PBO (t-PBO) fibers synthesized by a surface initiated polymerization (SIP) method. Interestingly, this OMAR phenomenon is capable of being tailored from positive

[a] *Shanghai Key Lab of Chemical Assessment and Sustainability, School of Chemical Science and Engineering, Tongji University, Shanghai 200092, People's Republic of China. E-mail: hongbogu2014@tongji.edu.cn*
[b] *Department of Chemistry & Biochemistry, Lamar University, Beaumont, TX, 77710, USA*
[c] *College of Chemical Engineering and Materials Science, Tianjin University of Science and Technology, Tianjin 300457, China*
[d] *Integrated Composites Lab (ICL), Department of Chemical & Biomolecular Engineering, University of Tennessee, Knoxville, TN, 37966, USA*
[e] *Key Laboratory of Materials Processing and Mold (Zhengzhou University), Ministry of Education, National Engineering Research Center for Advanced Polymer Processing Technology, Zhengzhou University, Zhengzhou, China*
[f] *Department of Physics and Astronomy, Louisiana State University, Baton Rouge, Louisiana, 70803, USA*
[g] *College of Chemical and Environmental Engineering, Shandong University of Science and Technology, Qingdao, Shandong 266590, China*
[h] *Henan Provincial Key Laboratory of Surface and Interface Science, Zhengzhou University of Light Industry, No. 136, Science Avenue, Zhengzhou, 450001, China*
[i] *College of Chemistry and Chemical Engineering, Henan University, Kaifeng 475004, China*

† Electronic supplementary information (ESI) available. See DOI: 10.1039/c9cc04789a

This journal is © The Royal Society of Chemistry 2019

Published on 09 July 2019. Downloaded on 9/26/2019 8:19:21 PM.

(up to 65.6% for a 10 wt% loading of t-PBO fibers) to negative (the maximum value is −34.8% for a 60 wt% loading of t-PBO fibers). Later on, we have explained this effect based on the paramagnetic nature of PBO molecules combined with the localization length a_0 calculated from the wave-function shrinkage model and the forward interference model.

The scarcity of functional groups on the surface of PBO fibers makes it difficult to adsorb anilines for further polymerization to form a PANI structure on the surface of PBO fibers. Since aniline can be easily adsorbed by acid functional groups on a substrate due to the electrostatic attraction, concentrated nitric acid (68.0–70.0 wt%) was used to treat the PBO fibers (named as t-PBO) as mentioned in the experimental section, ESI.† The acid treatment process does not significantly alter the thermal properties and structures of the PBO fibers as confirmed respectively in the TGA curves (the 10 wt% loss decomposition temperature for the t-PBO fibers is 624 °C, Fig. 1B-b, which is only a little bit lower than that of the as-received PBO fibers (635 °C), Fig. 1B-a), and SEM images in Fig. 2A and B (the surface of t-PBO is as smooth as the as-received PBO fibers without any obvious damage and the average diameter of the t-PBO fibers (around 11.5 μm) is similar to that of the as-received PBO fibers (approximately 12.0 μm), demonstrating the high structural stability of the PBO fibers). In addition, the acid treatment process favors the affinity of aniline to the t-PBO fibers, forming a uniform coating of PANI on the surface of the t-PBO fibers, Fig. 2C and D. On the contrary, the PANI coating cannot be achieved on the surface of as-received PBO fiber without acid treatment, Fig. S1A and B (ESI†), affirming the significance of acid treatment in the construction of PANI coated t-PBO fibers.

Moreover, in the FT-IR spectra of the as-received PBO (Fig. 1A-a) and t-PBO (Fig. 1A-b) samples, the peak at around 1620 cm^{-1} is attributed to the C=N stretching vibration of the benzoxazole ring.[23] The peak at around 1050 cm^{-1} corresponds to the =C–O–C stretching vibration.[24,25] The absorption peak at around 1700 cm^{-1}, as highlighted in the magenta rectangle, for the t-PBO fibers is assigned to the O–C=O stretching vibration in the carboxylic groups and is not obvious in the as-received PBO fibers, inset of Fig. 1A. The characteristic absorption peaks of pure PANI (1550, 1470, 1290, and 802 cm^{-1}),[26] Fig. 1A-c, are all observed in the PANI coated t-PBO fibers with different loadings of t-PBO fibers, verifying the presence of PANI on the surface of the t-PBO fibers. In addition, different from the as-received PBO fibers and the t-PBO fibers, in which the thermal decomposition mostly

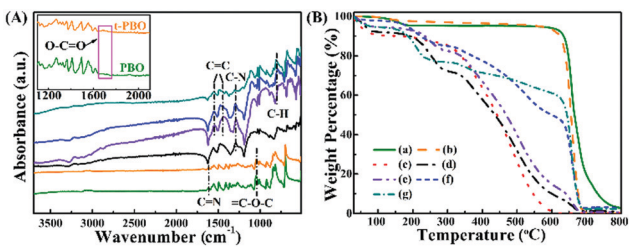

Fig. 1 (A) FT-IR spectra and (B) TGA curves for (a) PBO, (b) t-PBO, (c) pure PANI, and PANI coated t-PBO with a t-PBO loading of (d) 5, (e) 10, (f) 30, and (g) 60 wt%.

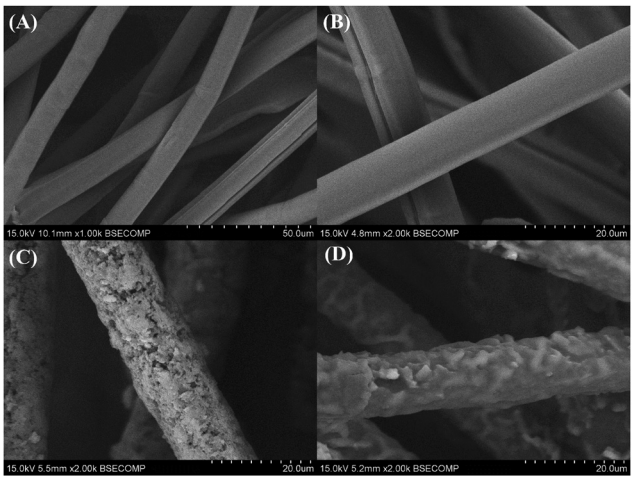

Fig. 2 SEM images of the (A) as-received PBO short fibers, (B) t-PBO short fibers, and PANI coated t-PBO fibers with a t-PBO loading of (C) 30 and (D) 60 wt%.

occurs within a very narrow temperature interval (around 650–700 °C), the PANI coated t-PBO fibers combine the degradation profiles of the t-PBO fibers and PANI together, exhibiting three weight loss stages corresponding to the elimination of moisture and dopant anions (from room temperature to 300 °C), thermal degradation of PANI (400–600 °C),[27] and decomposition of PBO (650–700 °C), as shown in Fig. 1B-d–g. The thermal stability of the t-PBO/PANI nanocomposites increases on increasing the t-PBO loading.

Furthermore, it turns out that the surface of the t-PBO fibers becomes rougher after the formation of the PANI coating and the PANI on the t-PBO fibers reveals a wrinkle-like microstructure, Fig. 2C, D and Fig. S2 (ESI†), compared with that of the as-received PBO and t-PBO (Fig. 2A and B) fibers. After decoration with PANI, the average diameter of the t-PBO fiber is respectively increased from 11.5 to 14.5, 14.0, and 12.5 μm for a t-PBO fiber loading of 5, 30, and 60 wt%.

The temperature dependent resistance of PANI covered t-PBO fibers with different t-PBO fiber loadings is measured from 100 to 290 K, Fig. 3A. In Fig. 3A, all the PANI coated t-PBO fibers exhibit a semiconducting behaviour within the measured temperature range and the resistance decreases with increasing temperature. Normally, the PBO fibers are insulating in nature and the electrical conductivity of PANI coated t-PBO fibers is dominated by the PANI layer. Consequently, a higher loading of t-PBO fibers, *i.e.*, a lower amount of PANI, leads to a higher resistance. The increased resistance is attributed to the fact that the insulating PBO can influence the interaction between PANI and doped acid PTSA, which partially blocks the charge transport pathway.[28]

To better investigate the electrical transport behaviour of PANI coated t-PBO fibers, the electrical conduction mechanism is elucidated from Fig. 3A using a variable range hopping (VRH) approach,[29] eqn (S1) (ESI†), which is represented as eqn (1):[29]

$$\sigma = \sigma_0 \exp\left[-\left(\frac{T_0}{T}\right)^{1/n+1}\right] \quad (1)$$

Published on 09 July 2019. Downloaded on 9/26/2019 8:19:21 PM.

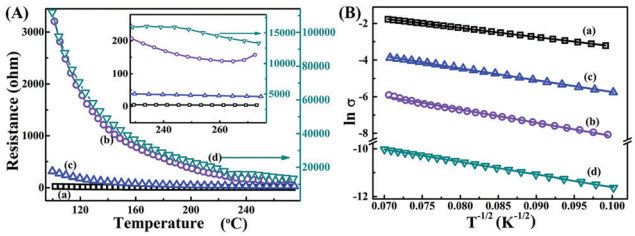

Fig. 3 (A) Resistance as a function of temperature, and (B) ln σ *vs.* $T^{-1/2}$ for the PANI coated t-PBO fibers with a t-PBO loading of (a) 5, (b) 10, (c) 30, and (d) 60 wt%.

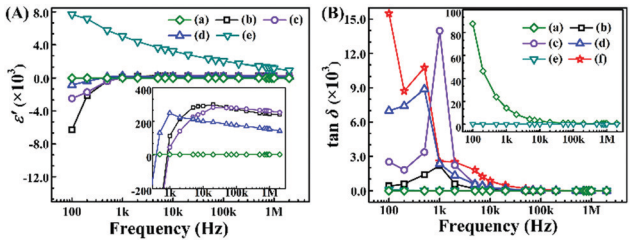

Fig. 4 (A) Frequency dependent real permittivity (ε') of (a) PBO fibers, and PANI coated t-PBO fibers with a t-PBO fiber loading of (b) 5, (c) 10, (d) 30, and (e) 60 wt%; (B) frequency dependent dielectric loss tangent (tan δ) for (a) PBO fibers, PANI coated t-PBO fibers with a t-PBO fiber loading of (b) 5, (c) 10, (d) 30, (e) 60 wt%, and (f) PANI.

where the constant σ_0 stands for the conductivity at the infinite low temperature, which includes tunnelling through the high barrier created by the organic capping layer and accounts for the attempt frequency of charge carriers trying to escape the nanocrystal; T (K) is the Kelvin temperature; and constant T_0 (K) is the Mott characteristic temperature, which is related to the energy needed for the hop of charge carriers.[29] In the VRH mechanism, Mott *et al.*[30] derived an $n = 3$ law for 3-d systems and Efros and Shklovskii (ES-VRH) showed that the density of states at the Fermi level ($N(E_F)$) vanishes quadratically at the Fermi level with an $n = 1$ law for 1-d systems after considering the Coulomb interaction. The best linear fit of $\ln(\sigma) \sim T^{-1/(n+1)}$ for each sample achieved from Fig. 3A is shown in Fig. 3B. The obtained $n = 1$ in the temperature range of 100–290 K indicates a quasi 1-d ES-VRH electrical conduction mechanism. The corresponding σ_0 and T_0 are listed in Table S1 (ESI†).

In this ES-VRH model, the characteristic temperature T_0 is predicted as $T_0 \approx 2.8e^2/4\pi\varepsilon\varepsilon_0 a_0 k_B$, where e is the electron charge, a_0 is the localization length, k_B is the Boltzman constant, ε is the permittivity of the material and ε_0 is the vacuum permittivity.[31,32] Normally, the permittivity refers to the nature of electrostatic energy savings and losses under the action of an alternative electric field and is usually expressed in terms of real permittivity (ε'), imaginary permittivity (ε'') and dielectric loss tangent (tan δ) and the corresponding results for PANI covered t-PBO fibers with t-PBO fiber loadings of 5, 10, 30, and 60 wt% and pure PANI within the frequency range of 100 Hz to 2 MHz at room temperature are shown in Fig. 4.[33,34] It is obvious that ε' of PBO is almost a constant with a value around 1.5, Fig. 4A-a, whereas PANI displays a negative permittivity over the measured frequency range especially at low frequencies (around -9.8×10^4 and -1.4×10^6, respectively), Fig. S5 (ESI†). As the t-PBO fiber loading rises from 5 to 30 wt%, ε' turns from negative to positive, Fig. 4A-b–d (refer to the inset of Fig. 4A). However, when the loading of t-PBO fibers is up to 60 wt%, the PANI coated t-PBO fibers exhibit a positive permittivity with a value from 7.7×10^3 to 9.2×10^2 over the measured frequency range. These results illustrate that the decoration of PANI on t-PBO fibers could control the permittivity of the t-PBO fibers. Generally, the peak in the dielectric loss (tan δ) curve is due to the resonance effect, in which the frequency of the system tends to oscillate with a larger amplitude than others, especially in materials with a negative permittivity. It turns out that PANI has a large tan δ peak with a value of around 1.1×10^4 at a low frequency of 500 Hz, whereas PBO possesses a very small tan δ value of appropriate 1.2×10^{-2}. As the loading of t-PBO fibers grows, similar to PANI, Fig. 4B-c–e, tan δ also shows a peak at a frequency that corresponds to the switching frequency, at which the permittivity changes from negative to positive, Fig. 4A-b–d. However, when the loading of t-PBO fibers increases to 60 wt%, the tan δ of the material is observed to exhibit a small value (about 87.7 at 100 Hz to 0.5 at 2 MHz) over the measured frequency range, Fig. 4C-f.

More interestingly, our PANI coated t-PBO fibers reveal a tunable MR property, in which the MR values can be altered by adding different loadings of t-PBO fibers. As displayed in Fig. 5 and Fig. S3 (ESI†), the MR value of pure PANI is up to 53.0% at a magnetic field of 9 T, Fig. S3-b (ESI†), whereas the MR for the PANI coated t-PBO fibers with a t-PBO fiber loading of 5, 10, 30, and 60 wt% is 1.2, 65.6, 5.1 and −34.8%, respectively. This may be due to the fact that the rigid-rod polymer PBO has an intrinsic paramagnetic property because of the existence of soliton and antisoliton as reported previously.[35] Generally, in a paramagnetic material (in which the material possesses unpaired electrons), each electron has a magnetic moment and spin angular momentum $S = 1/2$ with a spin quantum number of $m_s = +1/2$ and $m_s = -1/2$.[1] Upon exposure to a magnetic field H, the magnetic moment of the electron aligns itself either parallel ($m_s = -1/2$) or antiparallel ($m_s = +1/2$) to H, which is called the Zeeman effect and expressed as the equation: $E = m_s g_e \mu_B H$,[36] where m_s is the spin quantum number, g_e is the Zeeman g-factor, and μ_B is the Bohr magneton. In the absence of a magnetic field, due to the spin degeneracy, the two quantum states with spin quantum numbers of $m_s = +1/2$ and $m_s = -1/2$ are recognized to have the same energy level, whereas

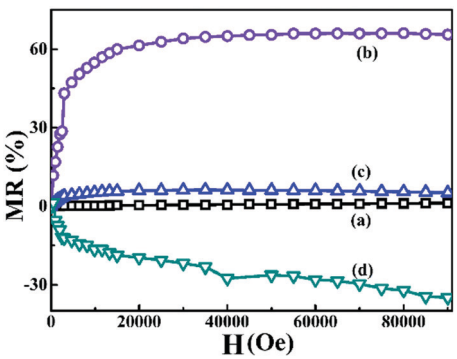

Fig. 5 Room temperature MR of PANI coated t-PBO fibers with a t-PBO loading of (a) 5, (b) 10, (c) 30, and (d) 60 wt%.

This journal is © The Royal Society of Chemistry 2019

Published on 09 July 2019. Downloaded on 9/26/2019 8:19:21 PM.

under a magnetic field separation between the upper and lower energy states takes place because $\Delta E = h\nu = g_e\mu_B H$ for the unpaired free electrons, in which $h\nu$ is the phonon energy relating to the frequency of the electromagnetic wave. After applying the magnetic field to the PANI coated t-PBO fibers, the electron spins in the paramagnetic PBO polymer could align with the magnetic field, leading to the resistance change of the PANI coated t-PBO fibers.

With the purpose of puzzling out this controllable OMAR effect in the PANI coated t-PBO fibers, the wave-function shrinkage model and forward interference model are introduced. Normally, in the VRH regime there is a parameter called a localization length (a_0) of the wave function for the localized charge carriers in the disordered system. The a_0 is related to the hopping distance R_{hop} by the expression $R_{hop} = (3/8)(T_0/T)^{1/4}a_0$. As reported previously,[11,12] the applied external magnetic field could result in a change of a_0, further leading to a change in the resistance of PANI and its nanocomposites. Since in our work the electrical transport mechanism confirms that our PANI coated t-PBO fibers follow the ES-VRH model, the wave-function shrinkage model is introduced to analyze the positive OMAR values and the forward interference model is exploited for the negative OMAR values as indicated in the supporting materials eqn (S1)–(S9) (ESI†) and the calculated a_0 at different magnetic fields is depicted in Table S2 (ESI†). It is concluded that when the OMAR value is positive, the a_0 is pretty small. For example, the a_0 for PANI coated t-PBO fibers with a 10 wt% loading of t-PBO fibers is 1.547, 0.718, and 0.536 nm for magnetic fields of 1, 5, and 9 T, respectively. However, as the OMAR value switches to negative for the PANI coated t-PBO fibers with 60 wt% t-PBO fibers, the a_0 is very large and is 348.664 nm at a magnetic field of 1 T. In this situation, the a_0 is meaningless for the negative OMAR, and the effect of interference among various hopping paths plays the important role.[37]

In summary, non-magnetic PANI coated poly (*p*-phenylene-2,6-benzobisoxazole) (PBO) fibers have demonstrated a controllable OMAR effect. The electrical transport mechanism of the PANI coated t-PBO fibers obeys a 1-d ES-VRH system. By integrating a positive dielectric constant of PBO and negative permittivity of PANI, the permittivity of PANI coated t-PBO fibers is altered from negative to positive. The OMAR effect of PANI coated t-PBO fibers changes from 1.2, 65.6, 5.1 to −34.8% for a t-PBO fiber loading of 5, 10, 30, and 60 wt%, respectively. The paramagnetic nature of the PBO fibers combined with the calculated a_0 from the wave-function shrinkage model and the forward interference model explain well this controllable OMAR effect in the PANI coated t-PBO fibers.

The authors are grateful for the support and funding from the National Natural Science Foundation of China (No. 51703165) and the Shanghai Rising-Star Program (No. 19QA1409400). This work is supported by the Shanghai Science and Technology Commission (14DZ2261100).

Conflicts of interest

There are no conflicts to declare.

Notes and references

1 H. Gu, X. Zhang, H. Wei, Y. Huang, S. Wei and Z. Guo, *Chem. Soc. Rev.*, 2013, **42**, 5907–5943.
2 M. Urdampilleta, S. Klyatskaya, J. P. Cleuziou, M. Ruben and W. Wernsdorfer, *Nat. Mater.*, 2011, **10**, 502–506.
3 P. Janssen, M. Cox, S. H. W. Wouters, M. Kemerink, M. M. Wienk and B. Koopmans, *Nat. Commun.*, 2013, **4**, 2286.
4 S. Han, G. Ma, S. Xie, W. Qin and S. Ren, *Org. Electron.*, 2018, **56**, 37–40.
5 M. Klein, S. Majumdar, P. Zassowski and W. Stampor, *J. Mater. Chem. C*, 2018, **6**, 482–490.
6 F. Ambrosio, J. Wiktor, F. De Angelis and A. Pasquarello, *Energy Environ. Sci.*, 2018, **11**, 101–105.
7 D. Casanova, *Chem. Rev.*, 2018, **118**, 7164–7207.
8 W. Wagemans, F. L. Bloom, P. A. Bobbert, M. Wohlgenannt and B. Koopmans, *J. Appl. Phys.*, 2008, **103**, 07F303.
9 (*a*) Y. Y. Ma, C. Hou, H. Zhang, Q. Zhang, H. Liu, S. Wu and Z. Guo, *Electrochim. Acta*, 2019, **315**, 114–123; (*b*) K. Gong, Q. Hu, Y. Xiao, X. Cheng, H. Liu, N. Wang, B. Qiu and Z. Guo, *J. Mater. Chem. A*, 2018, **6**, 11119–11128; (*c*) A. Berndt, J. Hwang and M. Islam, *et al.*, *Polymer*, 2019, **176**, 118–126.
10 (*a*) M. Liu, B. Li, H. Zhou, C. Chen, Y. Liu and T. Liu, *Chem. Commun.*, 2017, **53**, 2810–2813; (*b*) Y. Ma, M. Ma, X. Yin, Q. Shao, N. Lu, Y. Feng, Y. Lu, E. K. Wujcik, X. Mai, C. Wang and Z. Guo, *Polymer*, 2018, **156**, 128–135.
11 H. Gu, J. Guo, X. Yan, H. Wei, X. Zhang, J. Liu, Y. Huang, S. Wei and Z. Guo, *Polymer*, 2014, **55**, 4405–4419.
12 H. Gu, J. Guo, M. A. Khan, D. P. Young, T. D. Shen, S. Wei and Z. Guo, *Phys. Chem. Chem. Phys.*, 2016, 18, 19536–19543.
13 H. Gu, J. Guo, H. Wei, X. Zhang, J. Zhu, L. Shao, Y. Huang, N. Haldolaarachchige, D. P. Young, S. Wei and Z. Guo, *Polymer*, 2014, **55**, 944–950.
14 H. Gu, H. Zhang, J. Lin, Q. Shao, D. P. Young, L. Sun, T. D. Shen and Z. Guo, *Polymer*, 2018, **143**, 324–330.
15 M. Romero, R. Faccio, M. A. Tumelero, A. A. Pasa and A. W. Mombrú, *J. Mater. Chem. C*, 2017, **5**, 3779–3787.
16 J. Zhu, S. Wei, M. J. Alexander, T. D. Dang, T. C. Ho and Z. Guo, *Adv. Funct. Mater.*, 2010, **20**, 3076–3084.
17 Q. Ma, B. Wang, J. Lv, H. Li, B. Lei and C. Zhao, *Mater. Lett.*, 2017, **202**, 52–54.
18 Y. Tang, W. Dong, L. Tang, Y. Zhang, J. Kong and J. Gu, *Compos. Commun.*, 2018, **8**, 36–41.
19 T. Fukumaru, T. Fujigaya and N. Nakashima, *Macromolecules*, 2012, **45**, 4247–4253.
20 H. Chae and S. Kumar, *Science*, 2008, **319**, 908–909.
21 B. Jiang, K. Zhang, T. Zhang, Z. Xu and Y. Huang, *Compos. Part, B*, 2017, **121**, 1–8.
22 D. Liu, P. Chen, Q. Yu, K. Ma and Z. Ding, *Appl. Surf. Sci.*, 2014, **305**, 630–637.
23 L. Yang, M. Shi, J. Jiang, Y. Liu, C. Yan, H. Liu and Z. Guo, *Mater. Lett.*, 2019, **244**, 27–30.
24 F. Ran, X. Yang, X. Xu, Y. Bai and L. Shao, *Electrochim. Acta*, 2019, **301**, 117–125.
25 X. Yang, L. Yan, F. Ran, A. Pal, J. Long and L. Shao, *J. Membr. Sci.*, 2019, **576**, 9–16.
26 Q. Hu, N. Zhou, K. Gong, H. Liu, Q. Liu, D. Sun, Q. Wang, Q. Shao, H. Liu, B. Qiu and Z. Guo, *ACS Sustainable Chem. Eng.*, 2019, **7**, 5912–5920.
27 H. Gu, H. Zhang, C. Ma, S. Lyu, F. Yao, C. Liang, X. Yang, J. Guo, Z. Guo and J. Gu, *J. Phys. Chem. C*, 2017, **121**, 13265–13273.
28 Z. Cai, N. Zhang, M. Awais, A. Filatov and L. Yu, *Angew. Chem., Int. Ed.*, 2018, **57**, 6442–6448.
29 J. Xu, S. Li, Y. Bai and L. Shao, *J. Mater. Chem. A*, 2019, **7**, 10898–10904.
30 N. Mott and E. Davis, *Electronic Processes in Non-Crystalline Materials*, Oxford University Press, 2012, pp. 32–51.
31 H. Gu, X. Xu, M. Dong, P. Xie, Q. Shao, R. Fan, C. Liu, S. Wu, R. Wei and Z. Guo, *Carbon*, 2019, **147**, 550–558.
32 M. Khoshkhoo, Y. Joseph, S. Maiti, F. Schreiber, T. Chassé and M. Scheele, *Adv. Mater. Interfaces*, 2018, **5**, 1701623.
33 M. Verma and H. Sahu, *Ionics*, 2017, **23**, 1–12.
34 S. Wang and G. Dayton, *J. Am. Ceram. Soc.*, 1999, **82**, 2677–2682.
35 S. Wang, P. Guo, P. Wu and Z. Han, *Macromolecules*, 2004, **37**, 3815–3822.
36 J. Romero, H. Prima-Garcia, M. Varela, S. G. Miralles, V. Oestreicher, G. Abellán and E. Coronado, *Adv. Mater.*, 2019, **31**, 1900189.
37 H. Gu, J. Guo, Q. He, Y. Jiang, Y. Huang, N. Haldolaarachige, Z. Luo, D. P. Young, S. Wei and Z. Guo, *Nanoscale*, 2014, 6, 181–189.